JGR Oceans

RESEARCH ARTICLE
10.1029/2024JC021718

Kuroshio-Derived Anticyclonic Eddies Drive Lateral Transport and Transformation of Oceanic Dissolved Organic Matter Along the Continental Slope of South China Sea

Qinglong Liang[1], Chao Wang[2], Yan Li[3], Xufeng Xie[1], Xianghui Guo[1], Xin Liu[1], Weilei Wang[1], Zhisheng Zhang[2], and Weidong Guo[1,4]

[1]State Key Laboratory of Marine Environment Science, Xiamen University, Xiamen, China, [2]Laboratory for Coastal Ocean Variation and Disaster Prediction, College of Ocean and Meteorology, Guangdong Ocean University, Zhanjiang, China, [3]National Observation and Research Station for the Taiwan Strait Marine Ecosystem, Xiamen University, Xiamen, China, [4]College of Ocean and Earth Sciences, Xiamen University, Xiamen, China

Abstract Propagation of anticyclonic eddies (ACEs) facilitates the lateral transport of dissolved organic matter (DOM). However, the transformation of DOM within ACEs and its regulation of lateral fluxes of dissolved organic carbon (DOC) remain unclear. High-resolution sectional distribution of DOC and humic-like fluorescent DOM ($FDOM_H$) were investigated across a Kuroshio-derived ACE (K-ACE) on the slope of northern South China Sea (SCS). A two-endmember isopycnal mixing model revealed higher Kuroshio water fraction (0.59 ± 0.13) in K-ACE than non-eddy region. DOC removal (maximum 6%) was identified in the upper 200 m of K-ACE. The shallower mixed layer (<50 m) also revealed signals of $FDOM_H$ photobleaching (8%–34%). However, the substantial production of FDOMH (36%–43%) happened below the mixed layer (50–250 m). The regression slope between net $FDOM_H$ and apparent oxygen utilization in this layer was steeper in K-ACE than in non-eddy region and dark oceans, suggesting K-ACEs had higher microbial-mediated in situ production efficiency and rate of refractory DOM. This enhancement could be attributed to increased biogenic particle export, more Kuroshio-derived DOM transport, and higher oxygen utilization rate at warmer condition within K-ACE. Analysis of 27-year (1993–2020) daily eddy data revealed that K-ACE-induced lateral transport DOC flux to the northern SCS slope (1.8 ± 0.2 Tg C yr^{-1}) constitutes half of the external DOC flux via cross-shelf transport, highlighting the importance of K-ACEs in connecting carbon cycles between west Pacific and the northern SCS slope and even shelf areas.

Plain Language Summary The Kuroshio Current, originating from the tropical northwest Pacific, significantly influences the northern South China Sea's carbon cycle. This study explores its impact on dissolved organic matter via associated mesoscale anticyclonic eddies. Results show that a Kuoshio-derived anticyclonic eddy maintains a higher Kuoshio water fraction (~0.6) on the slope of northern South China Sea compared to surrounding waters. Enhanced production efficiency and rate of humic-like fluorophores was found in the eddy region in the lower euphotic and upper twilight layers compared to the non-eddy region, resulting in substantial production of refractory dissolved organic matter within the eddy. This enhancement is likely due to a combination of increased biogenic particles export, greater lateral transport of bioavailable dissolved organic matter by the Kuroshio, and higher oxygen utilization rate at higher temperature in the eddy region. An analysis of 27-year eddy data suggests that the Kuroshio-derived anticyclonic eddies might laterally transport about half of the dissolved organic carbon flux from coastal shelf to slope of the northern South China Sea, emphasizing the key role of eddy processes in linking carbon exchange between open oceans and marginal slopes and shelves.

1. Introduction

Marine DOM consists of complex components with varying geochemical reactivities ranging from labile to refractory, thereby dictating its photochemical and microbial transformation potential (Guo et al., 2012; Hansell, 2013; Mopper et al., 2015). In particular, humic-like FDOM ($FDOM_H$) can serve as a quantitative proxy for estimating the microbial production of deoxygenation-related refractory DOM (RDOM, Ogawa et al., 2001), owning to its strong correlation with apparent oxygen utilization (AOU). This transformation process has been

Qinglong Liang and Chao Wang are the co-first authors of the article.

Key Points:

- A higher Kuroshio fraction enhanced dissolved organic carbon (DOC) removal (<200 m) in a Kuroshio-derived anticyclonic eddy (ACE1) in the northern South China Sea
- Substantial production of humic-like fluorescent dissolved organic matter ($FDOM_H$) occurred in the upper twilight layer within ACE1
- ACE1 showed higher in situ production efficiency of $FDOM_H$ than non-eddy region and the deeper dark oceans

Supporting Information:

Supporting Information may be found in the online version of this article.

Correspondence to:

C. Wang and W. Guo,
chaowang@gdou.edu.cn;
wdguo@xmu.edu.cn

Citation:

Liang, Q., Wang, C., Li, Y., Xie, X., Guo, X., Liu, X., et al. (2025). Kuroshio-derived anticyclonic eddies drive lateral transport and transformation of oceanic dissolved organic matter along the continental slope of South China Sea. *Journal of Geophysical Research: Oceans*, *130*, e2024JC021718. https://doi.org/10.1029/2024JC021718

Received 14 AUG 2024
Accepted 28 JAN 2025

Author Contributions:

Conceptualization: Chao Wang, Yan Li, Weidong Guo
Funding acquisition: Weidong Guo
Investigation: Qinglong Liang, Xufeng Xie, Xianghui Guo, Xin Liu
Methodology: Chao Wang, Yan Li, Weilei Wang, Zhisheng Zhang
Software: Chao Wang, Weilei Wang, Zhisheng Zhang
Writing – original draft: Qinglong Liang, Chao Wang
Writing – review & editing: Chao Wang, Yan Li, Weidong Guo

widely observed across marginal seas and open oceans (Wang, Guo, et al., 2021; Yamashita & Tanoue, 2008) and contributes to the large carbon storage in the ocean interior (Carlson & Hansell, 2015). Till now, studies examining the production of $FDOM_H$ were mainly focused on the dark oceans (Catalá et al., 2015; Wang, Guo, et al., 2021). The upper twilight layer below the euphotic layer (150–300 m), characterized by approximately 60% remineralization of exported POC (Buesseler et al., 2020; Martin et al., 1987) and additional sources of labile organic materials (e.g., downward mixing of DOM, lateral advection, and daily migration of zooplankton), could be a potentially high productive layer for $FDOM_H$ (Giering et al., 2014). However, the in situ production efficiency of $FDOM_H$ ($E_{PR}(FDOM_H)$) in the upper twilight layer, which is sensitive to changing oceanic deoxygenation and RDOM sequestration (Jiao et al., 2024; Marsay et al., 2015), has not been well studied.

Mesoscale eddies, with well-known significant impacts on phytoplankton productivity in the euphotic layer and vertical export via the biological carbon pump (Omand et al., 2015; Xiu & Chai, 2011; Zhou et al., 2021), could also regulate lateral transport of DOC through propagation between the open ocean and coastal or marginal seas (McGillicuddy, 2016; Yamashita et al., 2024). This is especially important for anticyclonic eddies (ACEs) with longer lifetime and larger propagation distance than cyclonic eddies (CEs) (Chelton et al., 2011; Shi et al., 2024). These features, together with higher temperatures in ACEs than CEs, provide a favorable environment for potential microbial-mediated production of RDOC in the upper twilight layer along with eddy propagation. However, little is known about the quantification of lateral DOC transport, DOM transformations, and the related in situ production efficiency of RDOC.

ACEs generated during Kuroshio intrusion (hereafter K-ACEs) into the northern South China Sea (SCS) are common occurrences (Nan et al., 2015; Xiu et al., 2010). These K-ACEs propagate westward and may ultimately reach the continental slope and even shelf area (Qian et al., 2018), thus representing an important carbon exchange between open ocean and marginal seas (Wang, Xu, et al., 2021). In addition, a previous incubation experiment revealed enhanced biodegradation of Kuroshio-sourced DOM when intruding into the northern SCS by stimulating heterotrophic metabolism in the upper layer (Huang et al., 2019; Li et al., 2021). Thus, K-ACEs could be hotspots of DOM transformation influencing the production and sequestration of RDOC. Accordingly, this work presents high-resolution sampling of DOC and $FDOM_H$ in the upper 300-m layer along a transect crossing a K-ACE (ACE1) and the surrounding reference waters on the slope of northern SCS in spring 2020. Through integration of hydrographical, oxygen, nutrients, chlorophyll *a* (Chl *a*) data and an isopycnal mixing model, we quantified the transformation of DOC and $FDOM_H$ within ACE1 and along its eddy trajectory with a focus on the production of $FDOM_H$ in the upper twilight layer. Based on 27-year of daily eddy data (1993–2020), we also estimated the lateral transport flux of DOC by K-ACEs with the goal of understanding their potential long-term influence on the carbon budget of the northern SCS slope.

2. Materials and Methods

2.1. Field Observations and Identification of K-ACEs

Field observations were conducted aboard the R/V *Tan Kah Kee* from 15–20 April 2020 along a transect with 16 stations traversing the continental slope of the northern SCS (S1–S6 depth: 302–366 m; S7–S16 depth: 617–2,518 m) (Figure 1a). Additionally, station S, representing the SCS proper water endmember (Du et al., 2013), was investigated at the SCS basin. Vertical profiles of temperature, salinity, Chl *a*, and photosynthetically active radiation (PAR) were obtained at 16 stations using a calibrated SBE 911plus conductivity-temperature-depth unit and equipped with a calibrated Chl *a* fluorometer (WETLab, USA) and a LI-COR Biospherical PAR/Irradiance Sensor. The depth of the mixed layer was defined by a criterion of density change (Wang, Li, et al., 2021). Depth of euphotic zone at each daytime station was estimated by identifying the depth at which PAR was reduced to 1% of its surface value (Tseng et al., 2005). This depth was then defined as the upper boundary of the twilight zone.

Sea surface height from satellite altimeter data was monitored to track the propagation trajectory of ACE1 (Figure 1a). The range of this anticyclonic eddy during the observation period was determined by daily-averaged sea level anomaly (SLA) data from the Copernicus Marine Environmental Monitoring System (CMEMS) satellite altimeter (Figures 1b and 1c, available at: https://marine.copernicus.eu/). To obtain historical data on K-ACEs associated with the Kuroshio entering and dissipating in the northern SCS in nearly past 30 years (1 January 1993 to 7 March 2020), the mesoscale eddy trajectory data set META 2.0 DT provided by Archiving, Validation and Interpretation of Satellite Oceanographic (AVISO, https://www.aviso.altimetry.fr/en/data/products/value-added-products/global-mesoscale-eddy-trajectory-product/meta2-0-dt.html) was utilized. This data set, based on

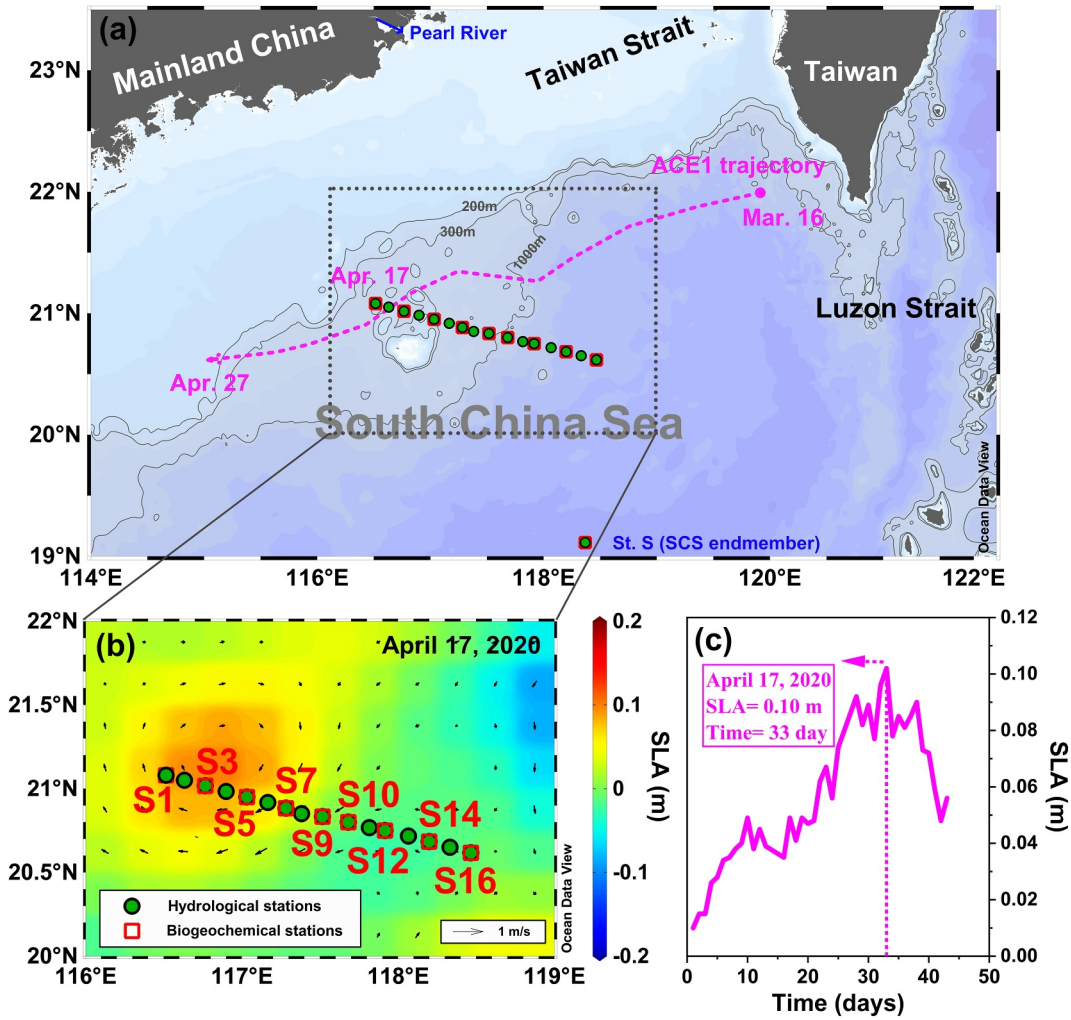

Figure 1. Map of the study area showing (a) trajectory of the anticyclonic eddy ACE1, (b) observation stations with sea level anomaly (SLA) and surface currents during ACE1 peak period, and (c) temporal changes in SLA associated with evolution of ACE1.

the SLA automatic eddy detection algorithm, covers mesoscale eddies with a lifespan exceeding 4 weeks and provides information on their radius, polarity, latitude, longitude, and date. Specifically, two types of K-ACEs were categorized based on their generation location: Type I at the Luzon Strait (120°E–122°E) and Type II in the west Pacific east of the Luzon Strait (east of 122°E) (Figure S1 in Supporting Information S1). K-ACEs that disappeared west of 121°E were identified as having entered the northern SCS (Table S1 in Supporting Information S1), whereas those that disappeared at water depths of <1,500 m were identified as approaching the slope of northern SCS (Table 1).

2.2. Sample Collection and Pretreatment

Water samples were collected at 10 biogeochemical stations (Figures 1a and 1b) using 10 L Niskin bottles attached to a rosette sampler. Sampling was conducted at nine depths within the upper 300 m, generally at 5, 15, 25, 50, 75, 100, 150, 200, and 300 m. Dissolved oxygen (DO) samples were collected in "turtleneck" glass bottles with ground glass stoppers and immediately fixed using manganese chloride and alkaline potassium iodide solution. Inorganic nutrient samples were filtered through MF-Millipore™ filters (pore size of 0.45 μm) and stored frozen until analysis. DOC and FDOM samples were filtered immediately through pre-combusted (500°C, 5 hr) GF/F filters into brown borosilicate glass vials with Teflon caps (Wang, Li, et al., 2021). The filters were stored frozen until analyzed for Chl *a* concentration. DOC samples were acidified to pH < 2 and stored frozen until

Table 1
Characteristics of Anticyclonic Eddies Approaching the Slope of Northern South China Sea Associated With Kuroshio Intrusion (1993–2020)

Type	Parameters	Spring	Summer	Autumn	Winter	Total
Type I[a]	Number	11	3	5	5	24
	Diameter (km)	100–241 (161 ± 56)	104–175 (132 ± 37)	86–258 (154 ± 66)	91–243 (141 ± 65)	86–258 (152 ± 56)
	Life cycle (day)	52–177 (94 ± 37)	32–150 (79 ± 63)	28–150 (77 ± 59)	33–94 (71 ± 25)	28–177 (84 ± 42)
Type II[b]	Number	1	0	0	1	2
	Diameter (km)	289	/	/	105	105–289 (197 ± 131)
	Life cycle (day)	175	/	/	33	33–175 (104 ± 100)

Note. "/" means no data. [a]Generation at the Luzon Strait. [b]Generation in the West Pacific east of Luzon Strait. Spring (March-May), Summer (June-August), Autumn (September-November), Winter (December-February).

analysis. FDOM samples were kept in the dark at −20°C until analysis within 1 week after the cruise (Spencer & Coble, 2014).

2.3. Analyses of DO, Nutrients, and Chl *a*

DO in water samples was measured on board with the Winkler titration method (Carpenter, 1965). Apparent oxygen utilization (AOU) was calculated as the difference between the calculated DO saturation concentration and the measured DO concentration (Schlitzer, 2023). The concentrations of nitrate (NO_3^--N) and soluble reactive phosphate (SRP) were analyzed onboard using a four-channel continuous flow Technicon AA3 Auto-Analyzer (Bran-Lube GmbH, Germany). The detection limits for both NO_3^--N and SRP were 0.03 μmol L^{-1} (Du et al., 2013). Chl *a* was extracted from samples using 90% aqueous acetone and kept in darkness at 4°C for 24 hr. The concentration of Chl *a* was then measured using a Turner Trilogy fluorometer (Welschmeyer, 1994). A strong linear relationship was found between Chl *a* concentrations measured by in situ fluorescence sensors and those obtained from extractable samples ($r = 0.85$, $n = 65$, $p < 0.0001$), allowing the sensor data to be used for generating high-resolution maps.

2.4. Analyses of DOC and $FDOM_H$

DOC concentrations were measured using a TOC-L_{CPH} analyzer (Shimadzu, Japan) in high temperature catalytic oxidation mode according to Wang, Li et al. (2021). A five-point standard curve was established daily using potassium hydrogen phthalate standards. The determination of DOC concentrations involved subtracting the running blank from the average peak area of samples (injected 3–5 times). The coefficient of variation for DOC analysis was approximately 2%. Low carbon water (LCW) and deep seawater reference (DSR) provided by D. A. Hansell's Lab from the University of Miami were routinely measured as quality control (https://hansell-lab.rsmas.miami.edu/consensus-reference-material/index.html).

Fluorescence excitation-emission matrices (EEMs) were obtained using an F-7100 spectrofluorometer (Hitachi, Japan) at room temperature (Wang, Guo, et al., 2021). Emission scans ranging from 280 to 600 nm were recorded at 2-nm intervals with excitation wavelengths ranging from 240 to 450 nm at 5-nm intervals. The EEMs were normalized and blank-corrected using daily Raman spectra of freshly generated Milli-Q water, and all data are presented in Raman Units (RU) (Lawaetz & Stedmon, 2009). To ensure comparability with previous results, three common humic-like components in marginal basins and open oceans (peak A, ex/em: 260/456 nm; peak C, ex/em: 355/456 nm and peak M, ex/em: 320/400 nm) were determined based on contour plots (Catalá et al., 2015; Coble, 1996; Jørgensen et al., 2011; Wang, Li, et al., 2021).

2.5. Two-Endmember Isopycnal Mixing Model Analysis

Based on potential temperature (θ)–salinity (Sal) plot (Figure 2a), the upper northern SCS exhibits two end-member water mass sources: Kuroshio (St. 74: 122.5°E, 20.0°N, Wang et al., 2017) and SCS (St. S, Figure 1a). Given the negligible diapycnal mixing (Du et al., 2013), a two-endmember isopycnal mixing model was employed to construct the conservative mixing scheme during the Kuroshio intrusion (Huang et al., 2019; Wang et al., 2017; Xu et al., 2018). The equations for a given water parcel in θ–Sal plot is defined as follows (Figure 2a):

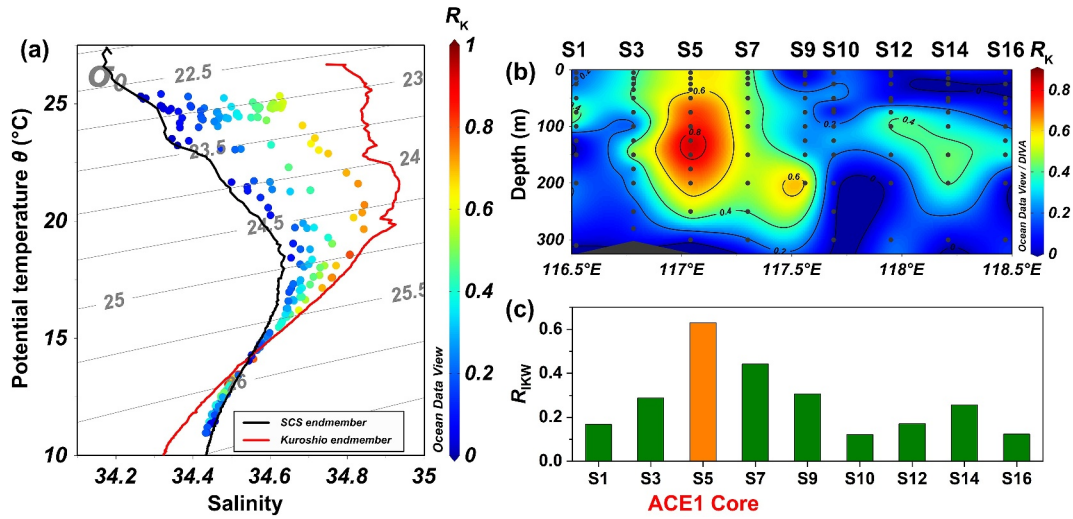

Figure 2. Isopycnal mixing model between Kuroshio endmember (St. 74: 122.5°E, 20.0°N, Wang et al., 2017) and SCS endmember (St. S: 118.5°E, 19.0°N). (a) Potential temperature-salinity diagram in the upper 300 m layer along the slope of northern South China Sea. The gray lines indicate the isopycnal line. (b) Sectional distribution of Kuroshio fraction (R_K). (c) Station-averaged Kuroshio fraction (R_{IKW}).

$$R_S + R_K = 1 \quad (1)$$

$$R_S \times \theta_S + R_K \times \theta_K = \theta \text{ or } R_S \times Sal_S + R_K \times Sal_K = Sal \quad (2)$$

Here, R_K and R_S represent the fractional contribution of Kuroshio or SCS endmember (Figure 2b). θ_S, θ_K and Sal_S, and Sal_K are potential temperature and salinity values for the SCS and Kuroshio endmember, respectively. θ and Sal denote the field-observed potential temperature and salinity for a given water sample. Salinity was adopted for R_K and R_S calculation in the upper 60 m due to its less sensitivity to seasonally varying heat flux. θ was used in the deeper water column (>60 m) because of higher sensitivity than salinity (Du et al., 2013). The R_K for a given station was integrated average over the upper 300 m to represent station-averaged Kuroshio water fraction (R_{IKW}, Figure 2c).

The net non-conservative biogeochemical alterations (Δ) of NO_3-N, DOC, and $FDOM_H$ (i.e., ΔNO_3-N, ΔDOC, and $\Delta FDOM_H$) during Kuroshio intrusion are thus defined as differences between field-observed and model-predicted values of these parameters (M):

$$M_{model-predicted} = M_K R_K + M_S R_S \quad (3)$$

$$\Delta M = M_{field-observed} - M_{model-predicted} \quad (4)$$

Here, M_S and M_K represent the values of NO_3^--N, DOC and $FDOM_H$ for the SCS endmember (St. S) and Kuroshio endmember. For the Kuroshio endmember, M_K values were sourced from St. 74 ($FDOM_H$) (Wang et al., 2017) or nearby stations (NO_3^--N: 122.5°E, 19.5°N, https://www.ncei.noaa.gov/products/world-ocean-atlas; DOC, 122.3°E, 20.0°N, Hansell et al., 2021). Comparison of data from various sources confirmed the applicability of the hydrological and chemical endmember values for Kuroshio water across different years or seasons (Text S1, Figure S2–S5 in Supporting Information S1). A perturbation test (conducted 50 times) was applied to evaluate the uncertainty in the isopycnal mixing model (Text S1, Lønborg & Álvarez-Salgado, 2014). The net production or consumption of organic material occurs along the isopycnal surface when ΔDOC or $\Delta FDOM_H$ is positive or negative, respectively (Wang et al., 2017; Wang, Guo, et al., 2021). ΔAOU values at depth range of 150–300 m, with little effect of air-sea exchange and photosynthesis on oxygen levels, were similarly calculated for indication of net oxygen consumption.

2.6. Statistical Analysis

The study evaluated the significance of hydrological, chemical, and DOM parameter differences using a two-tailed *t*-test with a significance level of 0.05 conducted in IBM SPSS Statistics 22.0.

3. Results

3.1. Evolution of ACE1 and Its Kuroshio Fraction

SLA data indicate the initiation of ACE1 to the southwest of Taiwan Island (119.9°E, 22.0°N) on 16 March 2020 (Figure 1a), thus belonging to Type I K-ACEs. Following its generation, ACE1 propagated southwestward along the slope of the northern SCS and reached its peak status 33 days later (SLA = 0.10 cm, 17 April 2020) northwest of the Dongsha Islands, a location (324 m depth) very close to the shelf break (Figures 1b and 1c). Continuing its westward propagation, ACE1 dissipated at the shallow shelf area (<200 m) on 27 April 2020, completing its lifecycle in 43 days (Figure 1c). The shedding period of ACE1 from the Kuroshio is consistent with previous observations, typically during the surface counter-clockwise circulation prevailing from November to April (Qian et al., 2018).

The Kuroshio water fraction (R_K) within the upper 300-m layer, as determined by the isopycnal mixing model, varied from 0.00 to 0.86 along the transect (Figure 2a). By integrating SLA and R_K values, water masses with $R_K > 0.4$ from stations S3 to S9 were identified as the ACE1 region (R_K: 0.59 ± 0.13) with S5 (0–250 m) as its core (R_K: 0.62 ± 0.21). The other water masses were categorized as western (R_K: 0.24 ± 0.15) and eastern (R_K: 0.15 ± 0.14) non-eddy regions (Figures 2b and 2c). High R_K values (>0.4) between 100–200 m from stations S12 to S16 likely do not originate directly from the Kuroshio Current due to lack of a subsurface high-salinity core (Wang et al., 2023). This signal can be attributed to the subduction of warmer water below 100 m (Figure 3a).

3.2. Sectional Distribution of Physical, Biological, and Chemical Parameters

Depth of the mixed layer ranged from 8 to 61 m and exhibited variations across the transect (Figure 3, Figure S6 in Supporting Information S1). Notably, the core of ACE1 had a deeper mixed layer (61 m) compared to the western (13–53 m) and eastern non-eddy region (8–54 m) ($p < 0.05$). Potential temperature (θ) decreased with depth with a downward concave isoline within the core of ACE1 (Figure 3a). The station-averaged θ of ACE1 in the 0–200 m depth exhibited a significantly higher value (21.0 C ± 0.6°C) compared to the non-eddy region (19.7 ± 0.9°C, $p < 0.01$). A well-developed subsurface salinity maximum from 75 to 200 m was also evident in ACE1 (Figure 3b). Both the maximum salinity and mean salinity throughout the upper 200-m water column were slightly higher in ACE1 (34.8 and 34.7 ± 0.06) compared to the non-eddy region (34.7 and 34.5 ± 0.02, $p < 0.01$). Remarkably, the salinity structure in the core of ACE1 closely resembled that of the Kuroshio from the western North Pacific (Nan et al., 2015).

The depth of euphotic zone at seven daytime stations (S1, S2, S9, S10, S12, S13, and S14) remained within a narrow range of 82–106 m, which was deeper than the mixed layer. The depth of the deep chlorophyll maximum (DCM) ranged between 46–72 m, falling between the depths of the mixed layer and euphotic zone (Figure S6 in Supporting Information S1). Notably, ACE1 consistently featured a deeper DCM compared to both the western and eastern non-eddy region (Figure 3c). Chl *a* concentration at the depth of DCM ranged from 0.56 μg L^{-1} at S9 station to 1.20 μg L^{-1} at S15 station (Figure S6 in Supporting Information S1). In contrast, the highest Chl *a* inventory (0–200 m) was observed at the periphery of ACE1 (S3 station, 80.3 mg m^{-2}), followed by S15 station (71.6 mg m^{-2}). Generally, the ACE1 displayed a lower Chl *a* inventory (37.8 mg m^{-2}) compared to the western non-eddy region (59.2 ± 8.8 mg m^{-2}) and the eastern non-eddy region (54.2 ± 11.0 mg m^{-2}) ($p < 0.01$). DO in the surface mixed layer was nearly saturated or slightly oversaturated, resulting in close to zero AOU values across all stations. Below the mixed layer, a notable decrease in AOU was observed in ACE1, contributing to the subduction of oxygen-rich surface water (Figure 3d). Similarly, the concentrations of station-averaged NO_3-N and SRP in the 0–200 m depth were significantly lower in ACE1 (4.5 ± 1.1 and 0.3 ± 0.1 μmol L^{-1}) compared to the non-eddy region (7.3 ± 1.2 and 0.5 ± 0.1 μmol L^{-1}, $p < 0.01$) (Figures 3e and 3f). The strong lineal correlation was found between NO_3^--N and SRP ($r = 0.999$, $p < 0.0001$, $n = 503$). Thus, for simplicity, only the NO_3^--N data were included in the following discussion.

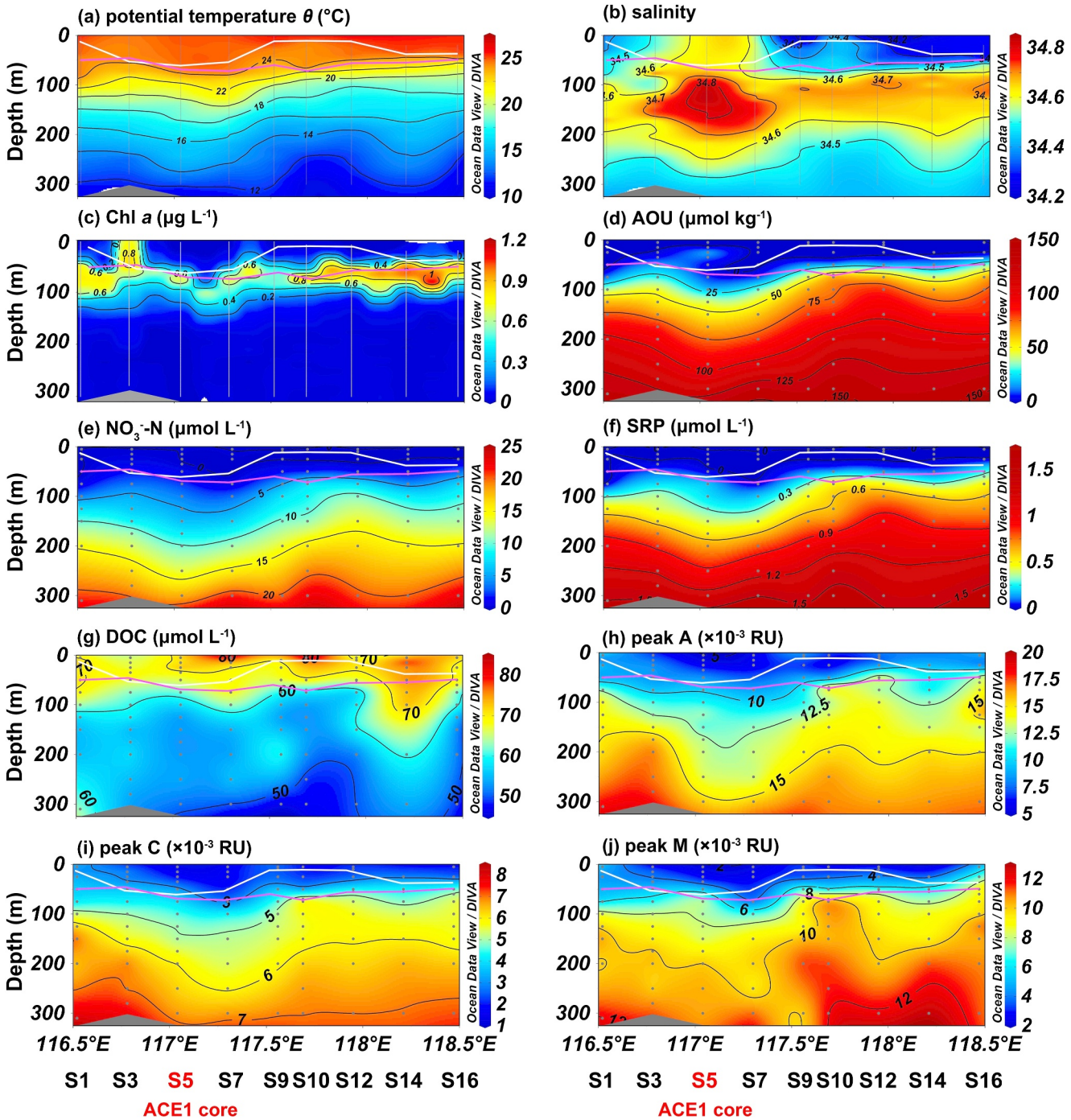

Figure 3. Sectional distribution of (a) potential temperature θ, (b) salinity, (c) Chl *a*, (d) AOU, (e) NO_3^--N, (f) SRP, (g) DOC, (h) peak A, (i) peak C, and (j) peak M on the slope of northern South China Sea. Depths of the mixed layer and deep chlorophyll maximum (DCM) are denoted by white and purple lines, respectively.

3.3. Sectional Distribution of DOC and $FDOM_H$

The DOC ranged from 45.8 to 81.6 μmol L^{-1} within the upper 300 m along the transect. It displayed a high and uniform distribution in the mixed layer, followed by a consistent decrease in the upper twilight layer (Figure 3g). Except for a notably higher DOC concentration at station S14, no significant differences in station-averaged DOC concentrations of the 0–200 m depth were observed between the ACE1 and non-eddy regions (61.0 ± 1.6 vs.

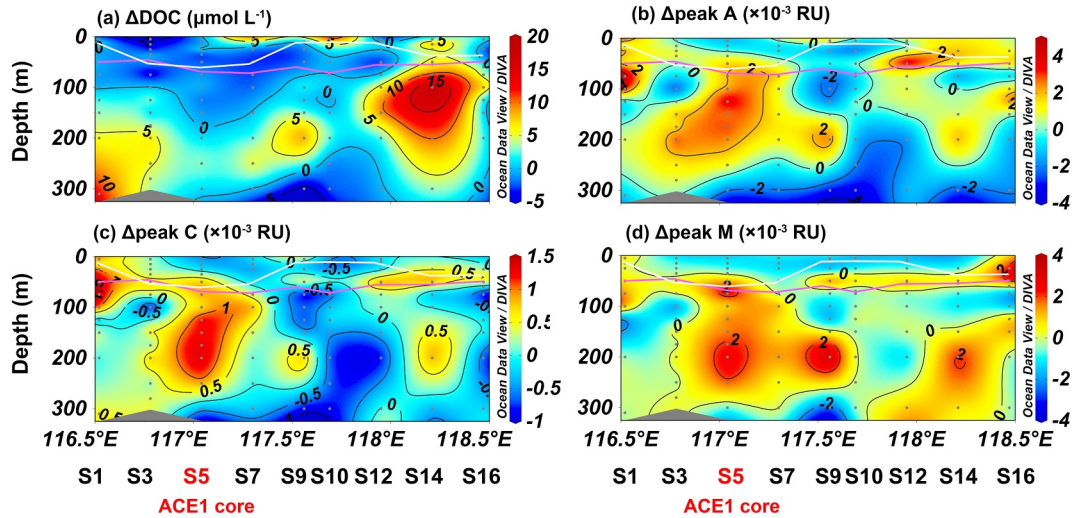

Figure 4. Sectional distribution of (a) ΔDOC and (b–d) $\Delta FDOM_H$ derived from a two-endmember isopycnal mixing model.

60.8 ± 1.2 μmol L^{-1}, Figure 2b; Figure S7a in Supporting Information S1). The intensities of humic-like peaks A, C and M showed a strong positive correlation in the upper 300 m ($r > 0.93$, $n = 95$, $p < 0.0001$) and negative relationships with DOC ($r < -0.76$, $n = 95$, $p < 0.0001$). The three $FDOM_H$ peaks exhibited low intensities in the mixed layer and rapidly increased with depth in the upper twilight layer. A distinct downwelling of $FDOM_H$-depleted waters was found in ACE1 (Figures 3h–3j) with station-averaged intensities (10.6 ± 1.0 RU for peak A, 4.2 ± 0.5 RU for peak C, 7.0 ± 0.6 RU for peak M) significantly lower than those in the non-eddy region (12.4 ± 0.7 RU for peak A, 5.0 ± 0.2 RU for peak C, 8.5 ± 0.6 RU for peak M; $p < 0.01$) but higher than those in the Kuroshio endmember ($p < 0.01$, Figures S7b–S7d in Supporting Information S1).

4. Discussion

4.1. Removal of DOC in the Upper Layer (0–200 m) of ACE1

Previous studies showed that DOC concentrations of the Kuroshio endmember were 15% higher than that of the SCS endmember (Figure S7 in Supporting Information S1, Wu et al., 2015; Li et al., 2021). Therefore, in the absence of biogeochemical changes during mixing of SCS and Kuroshio waters, the DOC concentration in the ACE1 should theoretically be higher than in the non-eddy region due to the higher proportion of Kuroshio water. Thus, the comparable DOC levels observed in the ACE1 and non-eddy region demonstrated that some DOC removal occurred within the K-ACEs (Figure 3g). To quantify this, we employed a routine isopycnal mixing model (Figure 2a). Positive ΔDOC and ΔDOC/DOC values (1.8 ± 4.6 μmol L^{-1} and 2.7 ± 7.1%) were observed in the non-eddy region particularly at stations between 118 and 118.5°E (Figure 4a). In these locations, elevated Chl *a* levels occurred at the DCM layer (Figure 3c), suggesting in situ production of DOC through phytoplankton productivity (Wu et al., 2017). Conversely, negative ΔDOC (−2.1 ± 1.1 μmol L^{-1}) and ΔDOC/DOC values (−3.5 ± 1.7%) were notable in ACE1 with a depth range of approximately 0–200 m (Figure 4a). RDOC comprises the majority of the total DOC pool even in the upper ocean due to its longer turnover time compared to water (>90%, Hansell et al., 2021). Moreover, Li et al. (2021) conducted a 45-day biodegradation experiment on surface Kuroshio DOM after its entry into the northern SCS and found only a 5 μmol L^{-1} loss of DOC (~6%). This value is consistent with our field-observed results, further confirming the credibility of a small but significant net DOC removal within the ACE1 compared to non-eddy region.

This observation implies that DOC degradation, coupled with Kuroshio intrusion, is not only confined to the northeast SCS basin near the Luzon Strait (east of 119°E) (Li et al., 2021). Instead, it may extend further westward near the northern SCS shelf brink (~116.5°E). A previous study revealed that stimulated heterotrophic metabolism reaches its peak status when the proportion of Kuroshio water is close to 50% (Huang et al., 2019). The proportion of Kuroshio water within the ACE1 in this study was 56%–86% (Figure 2b), thereby supporting the strong heterotrophic remineralization of DOM within the anticyclonic eddy. In addition, the incubation

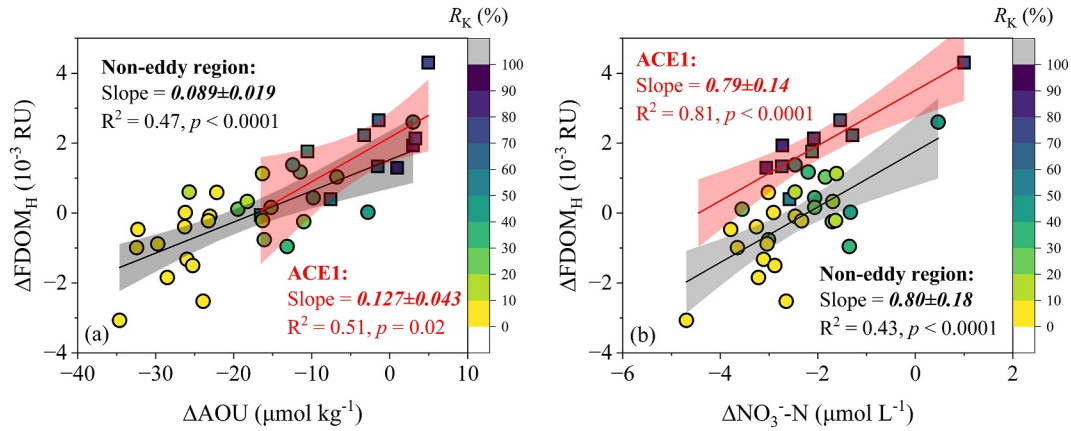

Figure 5. Relationships between $\Delta FDOM_H$ (represented by peak M) with ΔAOU, ΔNO_3^--N in anticyclonic eddy ACE1 (squares, 150–250 m) and non-eddy region (circles, 150–300 m). The color bar indicates the Kuroshio water fraction. The occurrence of negative $\Delta FDOM_H$, ΔAOU and ΔNO_3^--N values are possibly due to their low values in the premixing water masses compared to those in the endmembers of the mixing model.

experiment revealed up to 10% degradation of surface Kuroshio-derived DOC upon intrusion into the northern SCS following addition of nutrients (Li et al., 2021). This suggests that there is potential for further remineralization of Kuroshio-derived DOC when the ACE1 moves to the shelf of the northern SCS with higher nutrient levels (Du et al., 2021).

4.2. Removal of $FDOM_H$ in the Surface Mixed Layer (<50 m) and Addition in the Lower Euphotic and Upper Twilight Layers (50–250 m) Within ACE1

In the surface mixed layer (<50 m) of ACE1 with DOC removal, negative Δpeak A, Δpeak C, and Δpeak M were observed (hereafter $\Delta FDOM_H$) (Figures 4b–4d) with $\Delta FDOM_H/FDOM_H$ of −8.0 ± 14.1% for peak A, −12.5 ± 18.0% for peak C, and −33.7 ± 20.0% for peak M. Transformation of biodegradable DOM is usually accompanied by in situ $FDOM_H$ production (Qu et al., 2022; Xiao et al., 2023). Thus, the negative percentage of $\Delta FDOM_H/FDOM_H$ suggests the photobleaching of $FDOM_H$ in the shallower layer of ACE1 surpassed its production during long-distance transport (Guo et al., 2012; Yang et al., 2020), resulting in the lowest surface $FDOM_H$ intensity in the northern SCS (Wang et al., 2017).

In contrast, the positive $\Delta FDOM_H/FDOM_H$ values (36%–43%) in the lower euphotic and upper twilight layer of ACE1 (50–250 m) signify noticeable addition of $FDOM_H$ compared to the non-eddy region (−4.6 ± 10.5% for peak A, −4.1 ± 9.5% for peak C and −4.8 ± 11.9% for peak M). The refractory $FDOM_H$ is usually accumulated in the dark ocean (>200 m) (Catalá et al., 2015; Wang, Guo, et al., 2021; Yamashita & Tanoue, 2008). Our findings revealed that the Kuroshio-derived anticyclonic eddy could promote the production and accumulation of refractory carbon in the much shallower twilight layer. The positive relationships between $\Delta FDOM_H$ with ΔAOU and ΔNO_3^--N in the upper twilight layer provide additional confirmation that the in situ production of $FDOM_H$ is associated with microbial degradation of labile organic substrates accompanied by oxygen consumption and nutrient regeneration (Figure 5).

Compared with the notable increase of $FDOM_H$, degradation of Kuroshio-derived DOC in the 50–250 m layer of ACE1 was only 1.1 ± 2.8 μmol L^{-1}. Although a definitive DOC biodegradation experiment in ACE1 was not conducted to quantify the DOC removal/$FDOM_H$ production ratio, a dark incubation experiment focusing on terrigenous organic matter provides some clues (Xiao et al., 2022). The experiment demonstrated that a 1 mol L^{-1} removal of DOC could only support maximum additions of 2.6×10^{-4} RU and 7.3×10^{-4} RU for the humic-like peaks C and M, respectively. If we take this as a reference, the degradation of Kuroshio-derived DOC could not support the addition of $FDOM_H$ within ACE1. Alternatively, sinking of biogenic particles produced in situ emerge as a primary substrate for $FDOM_H$ production within ACE1. Although phytoplankton production in the

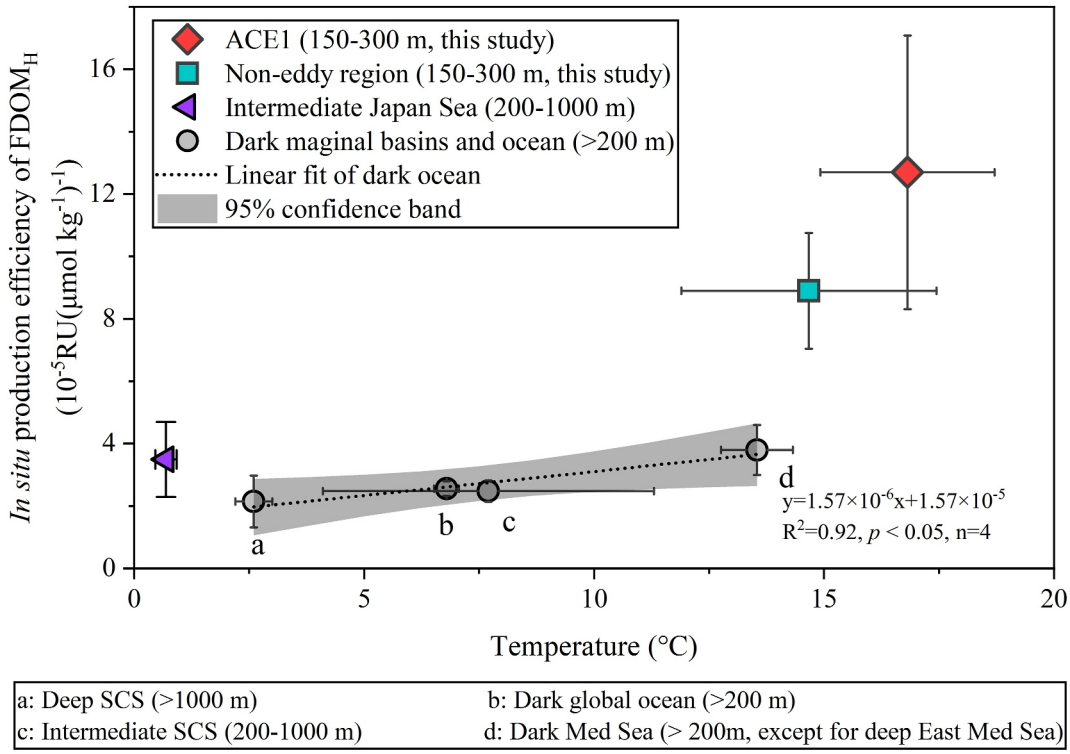

Figure 6. Comparison of in situ $FDOM_H$ production efficiency-temperature relationship between upper ACE1 and non-eddy region with dark oceans (Wang, Guo, et al., 2021). Data sources: Intermediate Japan Sea (Kim & Kim, 2016; Tanaka et al., 2014); Mediterranean (Med) Sea (Martínez-Pérez et al., 2019) and dark global ocean (Catalá et al., 2015).

ACE1 core was constrained by downward displacement of the nutricline (Figures 3e and 3f), elevated primary production was observed in the shallow layer of the eddy periphery (St. S3) (Figure 3c). A previous study found that strong water convergence in an anticyclonic eddy could transport biogenic POC into the eddy core enhancing its downward export (Zhou et al., 2013), thereby supporting subsequent microbial production of bio-refractory $FDOM_H$ in the upper twilight layer.

4.3. Anticyclonic Eddy Enhanced In Situ $FDOM_H$ Production Efficiency Versus Non-Eddy and Dark Oceans

Correlations between $\Delta FDOM_H$ and ΔAOU are commonly observed in the global dark open oceans and marginal seas (Catalá et al., 2015; Wang, Guo, et al., 2021). The regression slope ($\Delta FDOM_H/\Delta AOU$), that is, the production of $FDOM_H$ per unit of consumed oxygen, is indicative of the in situ production efficiency of refractory carbon (hereafter $E_{PR}(FDOM_H)$) (Catalá et al., 2015). A previous study reported a generally positive relationship between $E_{PR}(FDOM_H)$ and temperature across the dark marginal basins and global oceans (Wang, Guo, et al., 2021). This finding followed the classical Van't Hoff-Arrhenius relationship identifying temperature regulation of RDOM production rates.

It is clear that $E_{PR}(FDOM_H)$ in ACE1 was higher than in the non-eddy region and both were much higher than $E_{PR}(FDOM_H)$ in the dark oceans ($p < 0.05$) (Figure 6). The higher $E_{PR}(FDOM_H)$ in the upper twilight layer (150–300 m) than the dark oceans could be attributed to a substantially higher supply of labile/semi-labile substrates with a low apparent activation energy (Wang, Guo, et al., 2021). This corresponds to the fact that the storage of labile biogenic particles and DOC in the upper twilight layer of SCS was significantly greater than that in the dark SCS and global oceans with limited ventilation (Hansell, 2013; Kang et al., 2024). Similarly, higher $E_{PR}(FDOM_H)$ in the ACE1 than non-eddy region was due to enhanced supply of biogenic substrates (Zhou et al., 2013) and higher temperature (Figure 3a).

4.4. Contribution of K-ACEs on DOC Budget in the Slope of Northern SCS

The analysis of the historical AVISO data set shows that a total of 69 K-ACEs entered the northern SCS between 1993 and 2020 (Table S1 and Figure S1 in Supporting Information S1). Among these, 65 Type I K-ACEs showed a comparable average diameter (159 ± 58 km) but shorter lifetime (69 ± 35 days) than those of 4 Type II K-ACEs (154 ± 90 km, 96 ± 60 days) ($p < 0.05$). Eddy trajectories reveal that 24 Type I and 2 Type II K-ACEs annually and 14 Type I and 1 Type II K-ACEs during spring and summer had the potential to reach the slope of the northern South China Sea (bottom depth: 200–1,500 m) (Table 1).

To evaluate the intrusion of K-ACEs on the DOC budget of the slope of northern SCS, the DOC inventory within medium-sized ACE1 (i.e., diameter of 58 km) was quantified. First, we divided a series of boxes centered at each sampling depth in the upper 300-m water column for every station along the transect. The inventory of each box was calculated based on its volume, R_K fraction, and DOC concentration for the Kuroshio endmember at the same isopycnal layer. Then, the Kuroshio-derived DOC inventory of ACE1 on the slope of the northern SCS was estimated as ∼0.23 Tg C (Figure S8 in Supporting Information S1). If we assume the K-ACEs share the same source DOC profile and maintain the same R_K upon reaching the slope of SCS as ACE1, the estimated annual DOC flux approaching the slope of SCS is 1.8 ± 0.2 Tg C yr^{-1} (Figure S9a in Supporting Information S1). This value is half of the cross-shelf DOC flux onto the slope of SCS (∼3.1 Tg C, Meng et al., 2017). On a seasonal timescale, the estimated DOC flux by K-ACEs approaching the slope of SCS is 1.1 ± 0.1 Tg C yr^{-1} during spring and summer (March to August) (Figure S9b in Supporting Information S1). Thus, the K-ACE DOC transport flux is an important external carbon source to the northern SCS, as there was a net DOC export from the SCS to the West Pacific during the same seasons (Zheng et al., 2023). Daily eddy data and Argo profiles indicated that the average vertical extents of ACEs in the SCS could reach 400–500 m (He et al., 2018), demonstrating that K-ACE propagation to the slope of the northern SCS may provide a much higher DOC flux than current estimates. The enhanced remineralization of DOC (and also dissolved organic nitrogen; Xu et al., 2018) within K-ACEs suggests increased CO_2 production during eddy propagation. Given the longer lifetimes and more stable structure of ACEs compared to cyclonic eddies (Shi et al., 2024), this process could increase the export of inorganic carbon from the surface to subsurface SCS due to ACEs-induced downward transport (Figure S9 in Supporting Information S1). On the other hand, the enhanced production of $FDOM_H$ in the upper twilight layer indicates that K-ACEs could contribute to the storage of recalcitrant organic carbon in this system. These integrated processes result in anticyclonic eddies playing an important role in carbon sequestration of the northern SCS.

5. Implications

The global ocean is an important reservoir of RDOC (Hansell, 2013). Previous studies emphasize the importance of dark oceans especially the intermediate layer (200–1,000 m) in the production of RDOC (Catalá et al., 2015). However, our study found that the upper twilight layer has a greater supply of substrate and therefore higher $E_{PR}(FDOM_H)$. Furthermore, a warmer temperature in this layer stimulates a higher oxygen utilization rate (OUR). The combined results of these factors enhance the production rate of $FDOM_H$ (Wang, Guo, et al., 2021). Thus, the twilight layer plays a crucial role for RDOC production in the open oceans compared with the deeper dark oceans. These carbon pools could be an important source of RDOC when transported downward to the dark oceans (Roshan & DeVries, 2017). The higher $E_{PR}(FDOM_H)$ results in anticyclonic eddies becoming hotspots for RDOC production in open oceans. Additional studies of ACEs are required to confirm the extent of these carbon transformation processes, such as in the west Pacific which contains lot of K-ACEs (Wang, Li, et al., 2021). Based on a previous study (Wang, Guo, et al., 2021), the Q_{10} values for $E_{PR}(FDOM_H)$ in the intermediate SCS (200–1,000 m) and deep SCS (>1,000 m) were 1.74 and 1.85, respectively. The estimated Q_{10} value for the upper twilight layer of the transect in this study was not available due to limited data. Since this layer is quite sensitive to global warming (Meehl et al., 2011), future studies are needed to quantify the Q_{10} values in the upper twilight layers especially within the ACEs. Determination of Q_{10} values will allow for better characterization of the temperature sensitivity associated with production of bio-refractory carbon under future ocean warming conditions (Lønborg et al., 2020).

Data Availability Statement

Data are openly available in the Mendeley Data Repository via https://data.mendeley.com/datasets/2nyzr2rr7s/1 (Wang & Guo, 2024).

Acknowledgments
This research was funded by the National Natural Science Foundation of China (42276041, 41876083, and 41849906) and the National Key Research and Development Program of China (2022YFC3104805). Data and samples were collected onboard the R/V *Tan Kah Kee* during the open research cruise NORC2019-06. We thank Prof. Randy A. Dahlgren for his invaluable suggestions and Dr. Min Li, Ms. Xudong Shi for their assistance with data processing. The authors thank two anonymous reviewers for their insightful comments.

References

Buesseler, K. O., Boyd, P. W., Black, E. E., & Siegel, D. A. (2020). Metrics that matter for assessing the ocean biological carbon pump. *Proceedings of the National Academy of Sciences*, *117*(18), 9679–9687. https://doi.org/10.1073/pnas.1918114117

Carlson, C. A., & Hansell, D. A. (2015). Chapter 3 - DOM sources, sinks, reactivity, and budgets. In D. A. Hansell & C. A. Carlson (Eds.), *Biogeochemistry of marine dissolved organic matter* (2nd ed., pp. 65–126). Academic Press. https://doi.org/10.1016/B978-0-12-405940-5.00003-0

Carpenter, J. H. (1965). The Chesapeake Bay institute technique for the Winkler dissolved oxygen method. *Limnology & Oceanography*, *10*(1), 141–143. https://doi.org/10.4319/lo.1965.10.1.0141

Catalá, T. S., Reche, I., Fuentes-Lema, A., Romera-Castillo, C., Nieto-Cid, M., Ortega-Retuerta, E., et al. (2015). Turnover time of fluorescent dissolved organic matter in the dark global ocean. *Nature Communications*, *6*(1), 5986. https://doi.org/10.1038/ncomms6986

Chelton, D. B., Gaube, P., Schlax, M. G., Early, J. J., & Samelson, R. M. (2011). The influence of nonlinear mesoscale eddies on near-surface oceanic chlorophyll. *Science*, *334*(6054), 328–332. https://doi.org/10.1126/science.1208897

Coble, P. G. (1996). Characterization of marine and terrestrial DOM in seawater using excitation emission matrix spectroscopy. *Marine Chemistry*, *51*(4), 325–346. https://doi.org/10.1016/0304-4203(95)00062-3

Du, C., He, R., Liu, Z., Huang, T., Wang, L., Yuan, Z., et al. (2021). Climatology of nutrient distributions in the South China Sea based on a large data set derived from a new algorithm. *Progress in Oceanography*, *195*, 102586. https://doi.org/10.1016/j.pocean.2021.102586

Du, C., Liu, Z., Dai, M., Kao, S. J., Cao, Z., Zhang, Y., et al. (2013). Impact of the Kuroshio intrusion on the nutrient inventory in the upper northern South China Sea: Insights from an isopycnal mixing model. *Biogeosciences*, *10*(10), 6419–6432. https://doi.org/10.5194/bg-10-6419-2013

Giering, S. L. C., Sanders, R., Lampitt, R. S., Anderson, T. R., Tamburini, C., Boutrif, M., et al. (2014). Reconciliation of the carbon budget in the ocean's twilight zone. *Nature*, *507*(7493), 480–483. https://doi.org/10.1038/nature13123

Guo, W., Yang, L., Yu, X., Zhai, W., & Hong, H. (2012). Photo-production of dissolved inorganic carbon from dissolved organic matter in contrasting coastal waters in the southwestern Taiwan Strait, China. *Journal of Environmental Sciences*, *24*(7), 1181–1188. https://doi.org/10.1016/s1001-0742(11)60921-2

Hansell, D. A. (2013). Recalcitrant dissolved organic carbon fractions. *Annual Review of Marine Science*, *5*(1), 421–445. https://doi.org/10.1146/annurev-marine-120710-100757

Hansell, D. A., Carlson, C. A., Amon, R. M. W., Álvarez-Salgado, X. A., Yamashita, Y., Romera-Castillo, C., & Bif, M. B. (2021). Compilation of dissolved organic matter (DOM) data obtained from global ocean observations from 1994 to 2020 (NCEI Accession 0227166) [Dataset]. *NOAA National Centers for Environmental Information*. https://doi.org/10.25921/s4f4-ye35

He, Q., Zhan, H., Cai, S., He, Y., Huang, G., & Zhan, W. (2018). A new assessment of mesoscale eddies in the South China Sea: Surface features, three-dimensional structures, and thermohaline transports. *Journal of Geophysical Research: Oceans*, *123*(7), 4906–4929. https://doi.org/10.1029/2018JC014054

Huang, Y., Laws, E., Chen, B., & Huang, B. (2019). Stimulation of heterotrophic and autotrophic metabolism in the mixing zone of the Kuroshio Current and northern South China Sea: Implications for export production. *Journal of Geophysical Research: Biogeosciences*, *124*(9), 2645–2661. https://doi.org/10.1029/2018JG004833

Jiao, N., Luo, T., Chen, Q., Zhao, Z., Xiao, X., Liu, J., et al. (2024). The microbial carbon pump and climate change. *Nature Reviews Microbiology*, *22*(7), 408–419. https://doi.org/10.1038/s41579-024-01018-0

Jørgensen, L., Stedmon, C. A., Kragh, T., Markager, S., Middelboe, M., & Søndergaard, M. (2011). Global trends in the fluorescence characteristics and distribution of marine dissolved organic matter. *Marine Chemistry*, *126*(1–4), 139–148. https://doi.org/10.1016/j.marchem.2011.05.002

Kang, P., Ma, L., Zhang, H., Dai, X., Liu, J., Chen, W., & Tang, T. (2024). Amino acid carbon isotope profiles provide insight into lability and origins of particulate organic matter. *Limnology & Oceanography*, *69*(5), 1247–1259. https://doi.org/10.1002/lno.12567

Kim, J., & Kim, G. (2016). Significant anaerobic production of fluorescent dissolved organic matter in the deep East Sea (Sea of Japan). *Geophysical Research Letters*, *43*(14), 7609–7616. https://doi.org/10.1002/2016gl069335

Lawaetz, A. J., & Stedmon, C. A. (2009). Fluorescence intensity calibration using the Raman scatter peak of water. *Applied Spectroscopy*, *63*(8), 936–940. https://doi.org/10.1366/000370209788964548

Li, X., Wu, K., Gu, S., Jiang, P., Li, H., Liu, Z., & Dai, M. (2021). Enhanced biodegradation of dissolved organic carbon in the western boundary Kuroshio Current when intruded to the marginal South China Sea. *Journal of Geophysical Research: Oceans*, *126*(11), e2021JC017585. https://doi.org/10.1029/2021JC017585

Lønborg, C., & Álvarez-Salgado, X. A. (2014). Tracing dissolved organic matter cycling in the eastern boundary of the temperate North Atlantic using absorption and fluorescence spectroscopy. *Deep Sea Research Part I: Oceanographic Research Papers*, *85*, 35–46. https://doi.org/10.1016/j.dsr.2013.11.002

Lønborg, C., Carreira, C., Jickells, T., & Álvarez-Salgado, X. A. (2020). Impacts of global change on ocean dissolved organic carbon (DOC) cycling. *Frontiers in Marine Science*, *7*. https://doi.org/10.3389/fmars.2020.00466

Marsay, C. M., Sanders, R. J., Henson, S. A., Pabortsava, K., Achterberg, E. P., & Lampitt, R. S. (2015). Attenuation of sinking particulate organic carbon flux through the mesopelagic ocean. *Proceedings of the National Academy of Sciences*, *112*(4), 1089–1094. https://doi.org/10.1073/pnas.1415311112

Martin, J. H., Knauer, G. A., Karl, D. M., & Broenkow, W. W. (1987). VERTEX: Carbon cycling in the northeast Pacific. *Deep-Sea Research, Part A: Oceanographic Research Papers*, *34*(2), 267–285. https://doi.org/10.1016/0198-0149(87)90086-0

Martínez-Pérez, A. M., Catalá, T. S., Nieto-Cid, M., Otero, J., Álvarez, M., Emelianov, M., et al. (2019). Dissolved organic matter (DOM) in the open Mediterranean Sea. II: Basin-wide distribution and drivers of fluorescent DOM. *Progress in Oceanography*, *170*, 93–106. https://doi.org/10.1016/j.pocean.2018.10.019

McGillicuddy, D. J. (2016). Mechanisms of physical-biological-biogeochemical interaction at the oceanic mesoscale. *Annual Review of Marine Science*, *8*(1), 125–159. https://doi.org/10.1146/annurev-marine-010814-015606

Meehl, G. A., Arblaster, J. M., Fasullo, J. T., Hu, A., & Trenberth, K. E. (2011). Model-based evidence of deep-ocean heat uptake during surface-temperature hiatus periods. *Nature Climate Change*, *1*(7), 360–364. https://doi.org/10.1038/nclimate1229

Meng, F. F., Dai, M. H., Cao, Z. M., Wu, K., Zhao, X. Z., Li, X. L., et al. (2017). Seasonal dynamics of dissolved organic carbon under complex circulation schemes on a large continental shelf: The Northern South China Sea. *Journal of Geophysical Research: Oceans*, *122*(12), 9415–9428. https://doi.org/10.1002/2017jc013325

Mopper, K., Kieber, D. J., & Stubbins, A. (2015). Chapter 8. Marine photochemistry of organic matter. In D. A. Hansell & C. A. Carlson (Eds.), *Biogeochemistry of marine dissolved organic matter* (2nd ed., pp. 389–450). Academic Press. https://doi.org/10.1016/B978-0-12-405940-5.00003-0

Nan, F., Xue, H. J., & Yu, F. (2015). Kuroshio intrusion into the South China Sea: A review. *Progress in Oceanography*, *137*, 314–333. https://doi.org/10.1016/j.pocean.2014.05.012

Ogawa, H., Amagai, Y., Koike, I., Kaiser, K., & Benner, R. (2001). Production of refractory dissolved organic matter by bacteria. *Science*, *292*(5518), 917–920. https://doi.org/10.1126/science.1057627

Omand, M. M., D'Asaro, E. A., Lee, C. M., Perry, M. J., Briggs, N., Cetinic, I., & Mahadevan, A. (2015). Eddy-driven subduction exports particulate organic carbon from the spring bloom. *Science*, *348*(6231), 222–225. https://doi.org/10.1126/science.1260062

Qian, S. M., Wei, H., Xiao, J. G., & Nie, H. T. (2018). Impacts of the Kuroshio intrusion on the two eddies in the northern South China Sea in late spring 2016. *Ocean Dynamics*, *68*(12), 1695–1709. https://doi.org/10.1007/s10236-018-1224-y

Qu, L., He, C., Wu, Z., Dahlgren, R. A., Ren, M., Li, P., et al. (2022). Hypolimnetic deoxygenation enhanced production and export of recalcitrant dissolved organic matter in a large stratified reservoir. *Water Research*, *219*, 118537. https://doi.org/10.1016/j.watres.2022.118537

Roshan, S., & DeVries, T. (2017). Efficient dissolved organic carbon production and export in the oligotrophic ocean. *Nature Communications*, *8*(1), 2036. https://doi.org/10.1038/s41467-017-02227-3

Schlitzer, R. (2023). Ocean data view (Version 5.6.7) [Software]. *ODV*. https://odv.awi.de

Shi, W., Lin, H., Deng, Q., & Hu, J. (2024). Asymmetry of submesoscale instabilities in anticyclonic and cyclonic eddies. *Geophysical Research Letters*, *51*(2), e2023GL106853. https://doi.org/10.1029/2023GL106853

Spencer, R. G. M., & Coble, P. (2014). Chapter 4–Sampling design for organic matter fluorescence analysis. In P. Coble, J. Lead, A. Baker, D. M. Reynolds, & R. G. M. Spencer (Eds.), *Aquatic organic matter fluorescence* (pp. 125–146). Cambridge University Press. https://doi.org/10.1017/CBO9781139045452.008

Tanaka, K., Kuma, K., Hamasaki, K., & Yamashita, Y. (2014). Accumulation of humic-like fluorescent dissolved organic matter in the Japan Sea. *Scientific Reports*, *4*(1), 5292. https://doi.org/10.1038/srep05292

Tseng, C.-M., Wong, G. T. F., Lin, I.-I., Wu, C.-R., & Liu, K.-K. (2005). A unique seasonal pattern in phytoplankton biomass in low-latitude waters in the South China Sea. *Geophysical Research Letters*, *32*(8), L08608. https://doi.org/10.1029/2004GL022111

Wang, C., & Guo, W. (2024). Data supporting: Kuroshio-derived anticyclonic eddies drive lateral transport and transformation of oceanic dissolved organic matter along the continental slope of South China Sea (Version 1) [Dataset]. *Mendeley Data*. https://doi.org/10.17632/2nyzr2rr7s.1

Wang, C., Guo, W., Li, Y., Dahlgren, R. A., Guo, X., Qu, L., & Zhuang, W. (2021). Temperature-regulated turnover of chromophoric dissolved organic matter in global dark marginal basins. *Geophysical Research Letters*, *48*(19), e2021GL094035. https://doi.org/10.1029/2021GL094035

Wang, C., Guo, W. D., Li, Y., Stubbins, A., Li, Y. Z., Song, G. D., et al. (2017). Hydrological and biogeochemical controls on absorption and fluorescence of dissolved organic matter in the Northern South China Sea. *Journal of Geophysical Research: Biogeosciences*, *122*(12), 3405–3418. https://doi.org/10.1002/2017jg004100

Wang, C., Li, Y. Z., Li, Y., Zhou, H., Stubbins, A., Dahlgren, R. A., et al. (2021). Dissolved organic matter dynamics in the epipelagic northwest Pacific low-latitude western boundary current system: Insights from optical analyses. *Journal of Geophysical Research: Oceans*, *126*(9), e2021JC017458. https://doi.org/10.1029/2021jc017458

Wang, C. F., Xu, M. Q., Xuan, J., Li, H. B., Zheng, S., Zhao, Y., et al. (2021). Impact of the anticyclonic eddy on planktonic ciliate, with an emphasis on Tintinnids as bioindicator species. *Ecological Indicators*, *133*, 108441. https://doi.org/10.1016/j.ecolind.2021.108441

Wang, X. P., Du, Y., Zhang, Y. H., Wang, T. Y., Wang, M. Y., & Jing, Z. Y. (2023). Subsurface anticyclonic eddy transited from Kuroshio shedding eddy in the Northern South China Sea. *Journal of Physical Oceanography*, *53*(3), 841–861. https://doi.org/10.1175/jpo-d-22-0106.1

Welschmeyer, N. A. (1994). Fluorometric analysis of chlorophyll a in the presence of chlorophyll b and pheopigments. *Limnology & Oceanography*, *39*(8), 1985–1992. https://doi.org/10.4319/lo.1994.39.8.1985

Wu, K., Dai, M., Li, X., Meng, F., Chen, J., & Lin, J. (2017). Dynamics and production of dissolved organic carbon in a large continental shelf system under the influence of both river plume and coastal upwelling. *Limnology & Oceanography*, *62*(3), 973–988. https://doi.org/10.1002/lno.10479

Wu, K., Dai, M. H., Chen, J. H., Meng, F. F., Li, X. L., Liu, Z. Y., et al. (2015). Dissolved organic carbon in the South China Sea and its exchange with the western Pacific Ocean. *Deep Sea Research Part II: Topical Studies in Oceanography*, *122*, 41–51. https://doi.org/10.1016/j.dsr2.2015.06.013

Xiao, X., Powers, L. C., Liu, J., Gonsior, M., Zhang, R., Zhang, L., et al. (2022). Biodegradation of terrigenous organic matter in a stratified large-volume water column: Implications of the removal of terrigenous organic matter in the coastal ocean. *Environmental Science & Technology*, *56*(8), 5234–5246. https://doi.org/10.1021/acs.est.1c08317

Xiao, X., Yamashita, Y., Gonsior, M., & Jiao, N. (2023). The efficiency of the microbial carbon pump as seen from the relationship between apparent oxygen utilization and fluorescent dissolved organic matter. *Progress in Oceanography*, *210*, 102929. https://doi.org/10.1016/j.pocean.2022.102929

Xiu, P., & Chai, F. (2011). Modeled biogeochemical responses to mesoscale eddies in the South China Sea. *Journal of Geophysical Research*, *116*(C10), C10006. https://doi.org/10.1029/2010jc006800

Xiu, P., Chai, F., Shi, L., Xue, H., & Chao, Y. (2010). A census of eddy activities in the South China Sea during 1993–2007. *Journal of Geophysical Research*, *115*(C3), C03012. https://doi.org/10.1029/2009JC005657

Xu, M. N., Zhang, W., Zhu, Y., Liu, L., Zheng, Z., Wan, X. S., et al. (2018). Enhanced ammonia oxidation caused by lateral Kuroshio intrusion in the boundary zone of the northern South China Sea. *Geophysical Research Letters*, *45*(13), 6585–6593. https://doi.org/10.1029/2018GL077896

Yamashita, Y., Takekuma, T., Tajiri, M., Oida, J., Kakehi, S., Ooki, A., & Hirawake, T. (2024). Tracing sediment-affected water masses from coastal areas to offshore oceans using in situ sensing of fluorescent organic matter. *Journal of Geophysical Research: Oceans*, *129*(7), e2024JC020899. https://doi.org/10.1029/2024JC020899

Yamashita, Y., & Tanoue, E. (2008). Production of bio-refractory fluorescent dissolved organic matter in the ocean interior. *Nature Geoscience*, *1*(9), 579–582. https://doi.org/10.1038/ngeo279

Yang, F., Song, G., Massicotte, P., Wei, H., & Xie, H. (2020). Depth-resolved photochemical lability of dissolved organic matter in the western tropical Pacific Ocean. *Journal of Geophysical Research: Biogeosciences*, *125*(3), e2019JG005425. https://doi.org/10.1029/2019JG005425

Zheng, Y., Ma, W., Wang, Y., Liu, Z., & Xiu, P. (2023). Modeling dissolved organic carbon exchange across major straits and shelf breaks in the South China Sea. *Progress in Oceanography*, *210*, 102928. https://doi.org/10.1016/j.pocean.2022.102928

Zhou, K. B., Benitez-Nelson, C. R., Huang, J., Xiu, P., Sun, Z. Y., & Dai, M. H. (2021). Cyclonic eddies modulate temporal and spatial decoupling of particulate carbon, nitrogen, and biogenic silica export in the North Pacific Subtropical Gyre. *Limnology & Oceanography*, *66*(9), 3508–3522. https://doi.org/10.1002/lno.11895

Zhou, K. B., Dai, M. H., Kao, S. J., Wang, L., Xiu, P., Chai, F., et al. (2013). Apparent enhancement of ^{234}Th-based particle export associated with anticyclonic eddies. *Earth and Planetary Science Letters*, *381*, 198–209. https://doi.org/10.1016/j.epsl.2013.07.039

References From the Supporting Information

Huang, T. H., Chen, C. T. A., Tseng, H. C., Lou, J. Y., Wang, S. L., Yang, L., et al. (2017). Riverine carbon fluxes to the South China Sea. *Journal of Geophysical Research: Biogeosciences*, *122*(5), 1239–1259. https://doi.org/10.1002/2016jg003701